Single-particle states in spherical Si/SiO_2 quantum dots

A. S. Moskalenko* and J. Berakdar
Institut für Physik, Martin-Luther-Universität Halle-Wittenberg, Nanotechnikum-Weinberg, Heinrich-Damerow-Strasse 4, 06120 Halle, Germany
and Max-Planck-Institut für Mikrostrukturphysik, Weinberg 2, 06120 Halle, Germany

A. A. Prokofiev and I. N. Yassievich
Ioffe Physico-Technical Institute of RAS, 26 Polytechnicheskaya, 194021 St. Petersburg, Russia
(Received 15 January 2007; published 20 August 2007)

We calculate the ground and excited electron and hole levels in spherical Si quantum dots inside SiO_2 in a multiband effective mass approximation. The Luttinger Hamiltonian is used for holes, and the strong anisotropy of the conduction electron effective mass in Si is taken into account. As the boundary conditions for the electron and hole wave functions, we use the continuity of the wave functions and the flux at the boundaries of the quantum dots.

DOI: 10.1103/PhysRevB.76.085427 PACS number(s): 73.21.La, 73.22.Dj, 78.67.Hc, 78.60.−b

I. INTRODUCTION

The study of materials composed of Si nanocrystals dispersed in a SiO_2 matrix is an issue of high importance for various optoelectronic applications.[1,2] In particular, the knowledge of the energy spectrum of carriers confined in the nanocrystals and their wave functions is crucial for the understanding of electronic processes. Numerous theoretical works have dealt with the evaluation of the ground-state electron-hole pair energy of Si nanocrystals.[3–8] On the other hand, the problem concerning the energy-level positions and the corresponding eigenfunctions of the excited carrier states is studied much less.[9,10] However, shortly after the generation of an electron-hole pair in a nanocrystal, a number of important nonequilibrium processes involving these "hot" carriers may take place,[11] thus necessitating the knowledge of the excited states.

This current paper is devoted to the study of the ground and excited states of the electrons and holes within the framework of a multiband effective mass approximation. The finite energy barriers at the Si/SiO_2 boundary are explicitly accounted for. For the description of the electron and hole states of the carriers confined in Si nanocrystals, we utilize the envelope function approximation, taking into account the elliptic symmetry of the bottom of the conduction band and the complex structure of the top of the valence band in Si. The finite energy barriers at the boundary between Si and SiO_2 are treated by employing the Bastard boundary conditions.[12,13] This is the main difference between our method and earlier calculations based on the effective mass approximation[9] which failed to properly describe the optical properties of small nanocrystals. An advantage of our method in comparison with *ab initio* methods based on the density functional theory[5,8] is that, without a considerable numerical effort, we can calculate not only the ground state but also the excited states of the confined carriers. Furthermore, our theory is suitable for a broad range of nanocrystal sizes. We are not limited to nanocrystals with a small number of atoms.[49] Another point is that using the derived wave functions, the calculations of various excitation and deexcitation processes involving the confined carriers are transparent and allow for an insight into the underlying physics.

II. ELECTRON STATES

The conduction band of bulk Si has six equivalent minima in the first Brillouin zone at the points $\pm\vec{k}_{0,z}=(0,0,\pm 0.85)k_X$, $\pm\vec{k}_{0,y}=(0,\pm 0.85,0)k_X$, and $\pm\vec{k}_{0,x}=(\pm 0.85,0,0)k_X$, where $k_X=2\pi/a$ and $a=0.543$ nm is the lattice constant of Si.[14] The minima are situated in the neighborhood of the six X points (there are three nonequivalent X points). Assuming that the Bloch amplitudes are not changing in the neighborhood of the X point, one can write the wave function of one of the six equivalent ground states of electrons in the nanocrystal as

$$\psi_\nu^e = \xi^e(\vec{r})u_{c\nu}e^{i\vec{k}_{0,\nu}\vec{r}} \quad (\nu = \pm x, \pm y, \pm z). \tag{1}$$

$u_{c\nu}$ is one of two Bloch amplitudes of the bulk electron at the X point in the Brillouin zone, which corresponds to the lower conduction band at the $\vec{k}_{0,\nu}$ point. The envelope wave function ξ^e in Eq. (1) inside the Si quantum dot satisfies the following equation:

$$\frac{\hbar^2}{2m_\parallel}\frac{\partial^2}{\partial z^2}\xi^e(x,y,z) + \frac{\hbar^2}{2m_\perp}\left(\frac{\partial^2}{\partial x^2}+\frac{\partial^2}{\partial y^2}\right)\xi^e(x,y,z) + E\xi^e(x,y,z) = 0, \tag{2}$$

where $m_\parallel=0.916m_0$ and $m_\perp=0.19m_0$, with m_0 being the free electron mass. The rigorous formulation of the boundary conditions for the boundary between Si and SiO_2, in the framework of the envelope function method, is not a trivial task and generally has to be investigated in conjunction with experiment and numerical methods. The Bastard type boundary conditions imply that ξ and $\hat{\vec{v}}\xi$ are continuous across the boundary, where $\hat{\vec{v}}=\frac{1}{i\hbar}[\vec{r},\hat{H}]$ is the velocity operator, ξ is the envelope wave function, and $\hat{H}$ is the corresponding Hamiltonian.[12,13] Here, we assume that the spectrum of electronic states outside the nanocrystal in SiO_2 is isotropic and determined by a single electron effective mass which is equal to the free electron mass m_0. Then, outside the quantum dot, we have

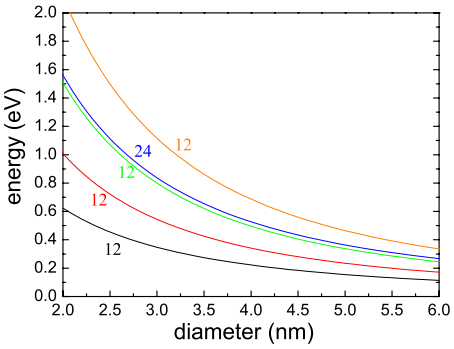

FIG. 1. (Color online) Dependence of positions of the electron energy levels above the bottom of the conduction band of bulk Si on the quantum dot diameter. The numbers near the lines indicate the total degeneracy (including the spin degeneracy) of the corresponding levels.

$$\frac{\hbar^2}{2m_0}\left(\frac{\partial^2}{\partial x^2}+\frac{\partial^2}{\partial y^2}+\frac{\partial^2}{\partial z^2}\right)\xi^e(x,y,z)+(E-U_e)\xi^e(x,y,z)=0, \tag{3}$$

where U_e is the energy barrier for electrons. According to Refs. 15 and 16, we have $U_e=3.2$ eV. The boundary conditions result in the following equations:

$$\xi^e|_{r=R_{\rm nc}^-}=\xi^e|_{r=R_{\rm nc}^+}, \tag{4}$$

$$\left[\frac{1}{m_\perp}\frac{\rho}{R_{\rm nc}}\frac{\partial\xi^e}{\partial\rho}+\frac{1}{m_\parallel}\frac{z}{R_{\rm nc}}\frac{\partial\xi^e}{\partial z}\right]_{r=R_{\rm nc}^-}=\left.\frac{1}{m_0}\frac{\partial\xi^e}{\partial r}\right|_{r=R_{\rm nc}^+}, \tag{5}$$

which are most conveniently written using the cylindrical coordinates ρ and z. Here, $R_{\rm nc}$ is the nanocrystal (nc) radius.

Equations (2) and (3) with the boundary conditions (4) and (5) have been solved numerically after separating the trivial angular part $\frac{1}{\sqrt{2\pi}}\exp(im\phi)$ $(m=0,\pm1,\pm2,\ldots)$ of the wave functions. A finite element numerical solver of the commercial package FLEXPDE was used for the numerical solution. Hence we obtain the electron energy levels and the corresponding envelope wave functions. The dependence of positions of the several lowest energy levels on the quantum dot diameter is depicted in Fig. 1. The dependence of the electron envelope wave functions on the distance from the center of the quantum dot is shown in Fig. 2 for $d=2$ nm (such a small diameter is chosen for demonstration reasons in order to resolve better the tunneling tails of the envelope wave functions). We have also compared the positions of the electron levels and their degeneracies with the existing data of Ref. 9, calculated by the empirical tight-binding method for quantum dots with diameter $d=7.61$ nm. We have found that apart from small level splittings due to the valley-orbit interaction neglected in our model, we get the same sequence of levels. The levels are, however, shifted toward the lower energies. The reason why we have smaller energies is that this tight-binding model used a truncation of Si nanocrystals by H atoms. This procedure is known to give higher energies and greatly overestimate the optical band gap when compared with experiments on Si/SiO_2 nanocrystals and recent *ab initio* time-dependent density functional theory calculations[8,17] as well as with our model.

III. HOLE STATES

For the description of the valence band structure in Si, we use a generalization of the Luttinger Hamiltonian[19] in the limit of vanishing spin-orbit coupling, which is justified for Si. That is, we write the Hamiltonian $\hat{H}$ in the form

$$\hat{H}=(A+2B)\hat{p}^2-3B(\hat{\vec{p}}\cdot\hat{\vec{J}})^2, \tag{6}$$

where $\hat{\vec{p}}$ is the momentum operator and $\hat{\vec{J}}$ is the unitary angular momentum operator acting in the space of Bloch amplitudes. Furthermore, we introduced

$$A=-\frac{1}{4}\frac{m_h+m_l}{m_h m_l}, \quad B=-\frac{1}{4}\frac{m_h-m_l}{m_h m_l}, \tag{7}$$

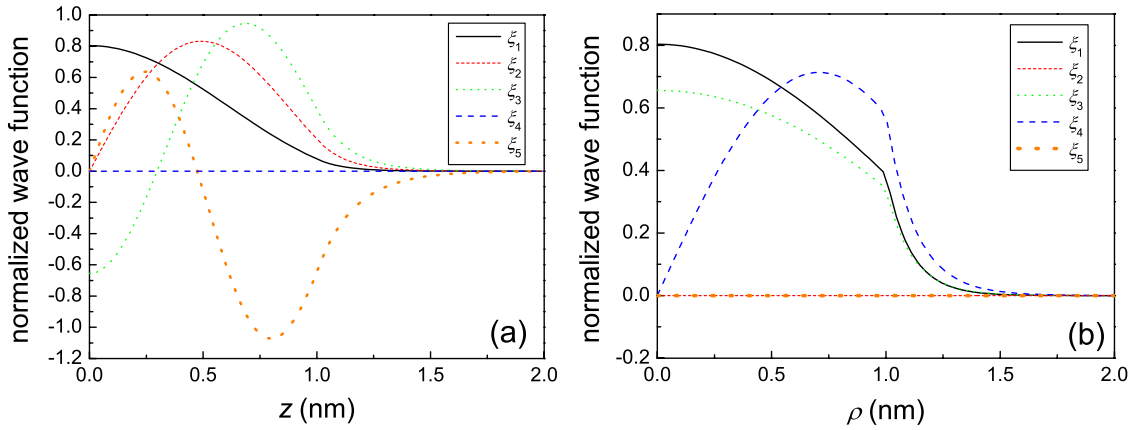

FIG. 2. (Color online) Electron wave function dependence on the cylindrical coordinates (a) z and (b) ρ for the lowest five electron levels of a quantum dot with diameter of 2 nm. The wave function ξ_4^e of the fourth level with magnetic number $m=\pm1$ has also an angular dependence $e^{im\phi}$.

$$m_h = \frac{m_0}{\gamma_1 - 2\gamma}, \quad m_l = \frac{m_0}{\gamma_1 + 2\gamma}, \quad \gamma = \frac{1}{5}(3\gamma_3 + 2\gamma_2). \quad (8)$$

Values of the constants γ_1, γ_2, and γ_3 for Si are 4.22, 0.53, and 1.38, respectively.[14] The basis of the Bloch amplitude space can be chosen in the form of spherical components[20] $u_0 = Z$, $u_\pm = \mp\sqrt{1/2}(X \pm iY)$ of the corresponding functions $X = yz$, $Y = xz$, and $Z = xy$ of the representation $\Gamma_{25'}$.[12,18]

In bulk Si, this model leads to two types of states corresponding to a doubly degenerate (in the absence of spin-dependent interactions) heavy hole band having mass m_h and a nondegenerate light hole band having mass $2m_h m_l/(3m_h - m_l)$. The quantum confinement gives rise to mixing of the states. Eigenfunctions of the Hamiltonian (6) can be found as eigenfunctions ψ_{FM} of the square $\hat{F}^2$ of the full angular momentum operator $\hat{\vec{F}} = \hat{\vec{L}} + \hat{\vec{J}}$ ($\hat{\vec{L}} = -i\vec{r} \times \partial_{\vec{r}}$; $\hat{\vec{L}}$ acts only on the envelope part of the wave function) and its projection $\hat{F}_z$ onto the axis z.[21] Eigenvalues of $\hat{F}^2$ and $\hat{F}_z$ are $F(F+1)$ and M, respectively, where $F = 0, 1, 2, \ldots$, and M can be any integer number having an absolute value no larger than F. For a spherical quantum dot, there are three types of states, namely,

$$\psi_{FM}^{F-1,F+1}(r,\theta,\phi) = R_F^{F-1}(r)\mathbf{Y}_{FM}^{F-1}(\theta,\phi) + R_F^{F+1}(r)\mathbf{Y}_{FM}^{F+1}(\theta,\phi), \quad (9)$$

$$\psi_{FM}^{F}(r,\theta,\phi) = R_F^{F}(r)\mathbf{Y}_{FM}^{F}(\theta,\phi), \quad (10)$$

$$\psi_{00}^{1}(r,\theta,\phi) = R_0^{1}(r)\mathbf{Y}_{00}^{1}(\theta,\phi), \quad (11)$$

where $R_F^{F-1}(r)$, $R_F^{F+1}(r)$, and $R_F^F(r)$ are the radial parts of the envelope wave functions. Furthermore,

$$\mathbf{Y}_{FM}^{L}(\theta,\phi) = \sum_{m_1,m_2} C_{Lm_1 1m_2}^{FM} Y_{Lm_1}(\theta,\phi) u_{m_2} \quad (12)$$

are the vector spherical harmonics that can be expressed in terms of the usual spherical harmonics $Y_{nm}(\theta,\phi)$ and the Clebsh-Gordon coefficients $C_{j_1 m_1 j_2 m_2}^{jm}$.[22] For the first two types of functions (9) and (10), only solutions with $F \geqslant 1$ are possible. We will see that the function (9) is of a mixed type, whereas functions (10) and (11) are of heavy and light hole types, respectively.

For a formulation of the boundary conditions for the hole states, we take into account that the main contribution to the valence band states in SiO_2 is given by p orbitals,[23] and for the description of the hole states outside the Si nanocrystal, we can use the same form of the Luttinger Hamiltonian (6). It is known that the hole masses at the valence band maximum in SiO_2 are pretty large.[23] For simplicity, we choose them to be equal to $m_v = 5m_0$. Then the corresponding values of the coefficients A_0 and B_0 of the Luttinger Hamiltonian (6) are $A_0 = -\frac{1}{2m_v}$ and $B_0 = 0$. In such a case, we can formulate appropriate Bastard type boundary conditions.

Inserting the functions $\psi_{FM}^{F-1,F+1}$ given by Eq. (9) into the Schrödinger equation with the Hamiltonian (6), we get the following equation system (see also Ref. 21) for the radial functions $R_F^{F-1}(r)$ and $R_F^{F+1}(r)$ inside the nanocrystal ($r < R_{nc}$):

$$\left(1 + \frac{F-1}{2F+1}\mu\right)\left[\frac{d^2}{dr^2} + \frac{2}{r}\frac{d}{dr} - \frac{(F-1)F}{r^2}\right]R_F^{F-1}(r) - \frac{3\sqrt{F(F+1)}}{2F+1}\mu\left[\frac{d^2}{dr^2} + \frac{2F+3}{r}\frac{d}{dr} + \frac{F(F+2)}{r^2}\right]R_F^{F+1}(r) = -\frac{E}{A\hbar^2}R_F^{F-1}(r), \quad (13)$$

$$-\frac{3\sqrt{F(F+1)}}{2F+1}\mu\left[\frac{d^2}{dr^2} - \frac{2F-1}{r}\frac{d}{dr} + \frac{(F-1)(F+1)}{r^2}\right]R_F^{F-1}(r) + \left(1 + \frac{F+2}{2F+1}\mu\right)\left[\frac{d^2}{dr^2} + \frac{2}{r}\frac{d}{dr} - \frac{(F+1)(F+2)}{r^2}\right]R_F^{F+1}(r) = -\frac{E}{A\hbar^2}R_F^{F+1}(r), \quad (14)$$

where E denotes the hole energy and $\mu = B/A$. The general solution of the system of equations given by Eqs. (13) and (14), which does not diverge at $r = 0$, is found as

$$R_F^{F-1}(r) = \mathcal{C} j_{F-1}(\lambda r/R_{nc}) + \mathcal{D} j_{F-1}(\lambda\beta r/R_{nc}), \quad (15)$$

$$R_F^{F+1}(r) = -\sqrt{\frac{F}{F+1}}\mathcal{C} j_{F+1}(\lambda r/R_{nc}) + \sqrt{\frac{F+1}{F}}\mathcal{D} j_{F+1}(\lambda\beta r/R_{nc}), \quad (16)$$

where $\mathcal{C}$ and $\mathcal{D}$ are coefficients to be found from the boundary and normalization conditions, $j_l(z)$ are the spherical Bessel functions of the first kind,[24] and

$$\beta = \sqrt{\frac{1-\mu}{1+2\mu}}. \quad (17)$$

The energy E, which is negative, is connected with the positive variable λ via

$$E = \frac{A\hbar^2}{R_{nc}^2}(1-\mu)\lambda^2 = -\frac{\hbar^2}{2m_h R_{nc}^2}\lambda^2. \quad (18)$$

Outside of the nanocrystal ($r > R_{nc}$), the radial parts of the functions $\psi_{FM}^{F-1,F+1}$ satisfy the following equations:

$$A_0\hbar^2\left[\frac{d^2}{dr^2} + \frac{2}{r}\frac{d}{dr} - \frac{(F-1)F}{r^2}\right]R_F^{F-1}(r) = -(E + U_h)R_F^{F-1}(r), \quad (19)$$

$$A_0\hbar^2\left[\frac{d^2}{dr^2} + \frac{2}{r}\frac{d}{dr} - \frac{(F+1)(F+2)}{r^2}\right]R_F^{F+1}(r) = -(E + U_h)R_F^{F+1}(r), \quad (20)$$

where U_h is the energy barrier for holes at the Si/SiO_2 boundary. Here, we take U_h=4.3 eV.[15,16] The general solution of the system of equations given by Eqs. (19) and (20), which converges to zero for large distances from the nanocrystal, is found as

$$R_F^{F-1}(r) = (\mathcal{C}_0 + \mathcal{D}_0) k_{F-1}(\kappa r/R_{\rm nc}), \tag{21}$$

$$R_F^{F+1}(r) = \left(-\sqrt{\frac{F}{F+1}}\mathcal{C}_0 + \sqrt{\frac{F+1}{F}}\mathcal{D}_0 \right) k_{F+1}\left(\frac{\kappa r}{R_{\rm nc}}\right), \tag{22}$$

where

$$\kappa = \frac{\sqrt{2m_v(E+U_h)}R_{\rm nc}}{\hbar}. \tag{23}$$

$\mathcal{C}_0$ and $\mathcal{D}_0$ are again coefficients to be found from the boundary and normalization conditions, and $k_l(z)$ are the modified spherical Bessel functions of the third kind.[24] The boundary conditions lead to the following equations for the radial functions:

$$R_F^{F-1}(r)\big|_{r=R_{\rm nc}^-} = R_F^{F-1}(r)\big|_{r=R_{\rm nc}^+}, \tag{24}$$

$$R_F^{F+1}(r)\big|_{r=R_{\rm nc}^-} = R_F^{F+1}(r)\big|_{r=R_{\rm nc}^+}, \tag{25}$$

$$\left\{ \left[\left(A + \frac{F-1}{2F+1}B \right)\frac{d}{dr} + \frac{3}{2}\frac{F-1}{2F+1}\frac{B}{r} \right] R_F^{F-1}(r) - \frac{3\sqrt{F(F+1)}}{2F+1} B \left(\frac{d}{dr} + \frac{F+2}{r} \right) R_F^{F+1}(r) \right\}_{r=R_{\rm nc}^-} = A_0 \left. \frac{d}{dr} R_F^{F-1}(r) \right|_{r=R_{\rm nc}^+}, \tag{26}$$

$$\left[-\frac{3\sqrt{F(F+1)}}{2F+1} B \left(\frac{d}{dr} - \frac{F-1}{r} \right) R_F^{F-1}(r) + \left[\left(A + \frac{F+2}{2F+1}B \right)\frac{d}{dr} + \frac{3}{2}\frac{F+2}{2F+1}\frac{B}{r} \right] R_F^{F+1}(r) \right]_{r=R_{\rm nc}^-} = A_0 \left. \frac{d}{dr} R_F^{F+1}(r) \right|_{r=R_{\rm nc}^+}. \tag{27}$$

Using the functions (15), (16), (21), and (22), in Eqs. (24)–(27) leads to a solvability condition determining the energy eigenvalues for states $\psi_{FM}^{F-1,F+1}$. We have derived this condition (see the Appendix). From it we have found numerically the energy eigenvalue dependence on the nanocrystal radius $R_{\rm nc}$. The corresponding coefficients $\mathcal{C}$, $\mathcal{D}$, $\mathcal{C}_0$, and $\mathcal{D}_0$, assuring the normalization condition, have also been derived numerically.

For the radial function $R_F^F(r)$ of the states ψ_{FM}^F, we get the following equation inside the Si quantum dot:

$$(1-\mu)\left[\frac{d^2}{dr^2} + \frac{2}{r}\frac{d}{dr} - \frac{F(F+1)}{r^2} \right] R_F^F(r) = -\frac{E}{A\hbar^2} R_F^F(r). \tag{28}$$

One can easily see that it is the same equation as for the radial part of the wave function of a particle having a simple parabolic band with a heavy hole mass and angular momentum F. For the radial function $R_0^1(r)$ of the states ψ_{00}^1, we get

$$(1+2\mu)\left[\frac{d^2}{dr^2} + \frac{2}{r}\frac{d}{dr} - \frac{2}{r^2} \right] R_0^1(r) = -\frac{E}{A\hbar^2} R_0^1(r). \tag{29}$$

This equation is then the same as for a simple particle having a light hole mass and angular momentum 1. Solving Eqs. (28) and (29), we find

$$R_F^F(r) = \mathcal{C}' j_F(\lambda r/R_{\rm nc}), \tag{30}$$

$$R_0^1(r) = \mathcal{C}'' j_1(\lambda\beta r/R_{\rm nc}), \tag{31}$$

for $r < R_{\rm nc}$, where $\mathcal{C}'$ and $\mathcal{C}''$ are the corresponding normalization coefficients. Outside the nanocrystal, $R_F^F(r)$ satisfies the equation

$$A_0\hbar^2\left[\frac{d^2}{dr^2} + \frac{2}{r}\frac{d}{dr} - \frac{F(F+1)}{r^2} \right] R_F^F(r) = -(E+U_h) R_F^F(r), \tag{32}$$

and $R_0^1(r)$ satisfies the equation

$$A_0\hbar^2\left[\frac{d^2}{dr^2} + \frac{2}{r}\frac{d}{dr} - \frac{2}{r^2} \right] R_0^1(r) = -(E+U_h) R_0^1(r). \tag{33}$$

Solutions which have an appropriate behavior at infinity are

$$R_F^F(r) = \mathcal{C}_0' k_F(\kappa r/R_{\rm nc}), \tag{34}$$

$$R_0^1(r) = \mathcal{C}_0'' k_1(\kappa r/R_{\rm nc}). \tag{35}$$

The boundary conditions in this case are found as

$$R_F^F(r)\big|_{r=R_{\rm nc}^-} = R_F^F(r)\big|_{r=R_{\rm nc}^+}, \tag{36}$$

$$\left[(A-B)\frac{d}{dr} - \frac{3}{2}\frac{B}{r} \right] R_F^F(r)\Big|_{r=R_{\rm nc}^-} = A_0 \left. \frac{d}{dr} R_F^F(r) \right|_{r=R_{\rm nc}^+}, \tag{37}$$

for $R_F^F(r)$ functions, and

$$R_0^1(r)\big|_{r=R_{\rm nc}^-} = R_0^1(r)\big|_{r=R_{\rm nc}^+}, \tag{38}$$

$$\left[(A+2B)\frac{d}{dr} + \frac{3B}{r} \right] R_0^1(r)\Big|_{r=R_{\rm nc}^-} = A_0 \left. \frac{d}{dr} R_0^1(r) \right|_{r=R_{\rm nc}^+}, \tag{39}$$

for $R_0^1(r)$ functions. Using the form of the radial wave functions given by Eqs. (30) and (34) [Eqs. (31) and (35)] in Eqs. (36) and (37) [Eqs. (38) and (39)], we get the equation determining the energy levels of states ψ_{FM}^F [ψ_{00}^1] (see the Appendix). Solving this equation numerically, we found the

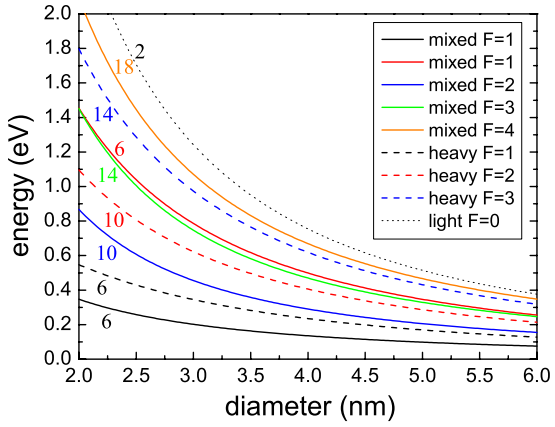

FIG. 3. (Color online) Dependence of the positions of the hole energy levels below the top of the valence band of bulk Si on the quantum dot diameter. The numbers near the lines indicate the total degeneracy (including the spin degeneracy) of the corresponding levels. The types of the levels and values of the total angular momentum F are also shown.

energy-level positions of holes of the heavy and light hole types.

The dependence of positions of the hole energy levels on the nanocrystal radius, their types, and degeneracies are presented in Fig. 3 for the lowest few hole levels. One can see that the hole level structure is denser in comparison with the electron level structure. This can lead to important differences in behavior between hot electrons and holes.[25]

IV. COULOMB SHIFT

The Coulomb interaction leads to a decrease in the recombination energy of an electron-hole pair.[26] This interaction should be considered while taking into account the "image charge" effects appearing because of the dielectric constant difference at the quantum dot boundary. On the other side, the dielectric constant mismatch leads to the interaction of a charged particle with its own image. The resulting polarization self-energy correction increases single-particle energies of electrons and holes (counted upward from the bottom of the bulk conduction band and downward from the top of the valence band, respectively). If the dielectric constant changes discontinuously at the quantum dot boundary, the polarization self-interaction diverges there. This is not an immediate problem for models of quantum dots assuming infinite energy barriers for electrons and holes at the quantum dot boundary, because particle wave functions vanish there and the self-energy correction induced by the self-interaction remains finite.[27–29] However, as a consequence of the finite energy barriers, the particle wave functions are finite at the quantum dot boundary (see Fig. 2) and self-energy corrections become infinite.

In order to remove these unphysical divergences, one has to take into account that the position-dependent dielectric constant should change smoothly between the values corresponding to the quantum dot core and the surrounding material on the scale of the interatomic distance. This can be done

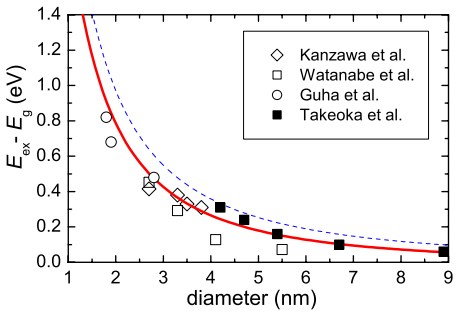

FIG. 4. (Color online) Dependence of the ground-state electron-hole recombination energy as a function of diameter of nanocrystal (solid line). The dashed line shows the same energy without taking into account the exciton shift. For comparison, the experimental data obtained from photoluminescence spectra (Refs. 37–40), measured for Si nanocrystals inside SiO_2, are presented.

in a simple and an intuitive way by "regularizing" directly the self-interaction.[30,31] A more physical and controllable, though also more demanding, way is to solve the inhomogeneous problem with the smooth position-dependent dielectric constant.[32] Calculations of Ref. 32 show that the total correction to the electron-hole pair energy introduced by the Coulomb and image charge interactions depends strongly on the width of the transition region between two values of the dielectric constant. For reasonable values of the transition region width around the interatomic distance, the corrections introduced by the electron-hole Coulomb interaction and the polarization self-energy corrections cancel each other to a large extent. Therefore, the overall Coulomb correction to the energy of the electron-hole pair is small, and electron-hole recombination energy is pretty accurately given by the sum of the band gap with the electron and hole single-particle quantization energies. This conclusion is also supported by *ab initio* and tight-binding calculations for small hydrogen-terminated silicon nanocrystals.[33] The excitonic effects may be more significant for small nanocrystals with diameters smaller than 2 nm.[34,35]

An estimate (rather an upper limit estimate[32]) of the overall Coulomb shift V_C can be deduced using single-particle wave functions corresponding to infinitely high energy barriers. We have calculated V_C under these assumptions, treating the Coulomb correction as a perturbation to the single-particle Hamiltonian.[29,36] The result for the ground-state electron and hole can be given then in a simple form: $V_C = -1.54e^2/(\kappa_{Si}R_{nc})$, where κ_{Si} is the dielectric constant of Si and it was taken into account that the surrounding material has a dielectric constant approximately three times smaller than Si (one should notice that Ref. 29 gives a different numerical constant computed incorrectly by us). The excitonic shift calculated in the same way for higher states of electrons and holes is of the same order and smaller.

In Fig. 4, the dependence of the exciton energy as a function of the nanocrystal diameter is presented for the ground state. This dependence is also shown when the excitonic energy shift is accounted for. The theory is compared with the experimental data obtained from the photoluminescence spectra.[37–40] We should remark that by calculating the carrier

levels and the ground-state exciton energy, the strain effects induced by the boundary between Si and SiO_2 were neglected. These effects may become important for small nanocrystals.[17,41]

V. RADIATIVE RECOMBINATION

We have calculated the probabilities P_r of radiative recombination assisted by emission of an optical transverse phonon (with energy 57.5 meV) as well as a longitudinal one (55.3 meV). These channels of radiative transitions dominate in bulk Si.

The probability of a spontaneous radiative transition of an electron from the initial state i (electron state), with energy E_i, to the final state f (hole state), with energy E_f, assisted by emission of a phonon with frequency ω_0 can be found using second order perturbation theory. In the framework of this theory, the process goes via a virtual state j having energy E_j. Then the probability of emitting a photon with frequency $\omega=(E_i-E_f)/\hbar-\omega_0$ into the angle $d\Omega$ per time unit is given by

$$P_r^{fi}d\Omega=\left(\frac{e}{m_0c}\right)^2\frac{\omega n_{\text{eff}}}{2\pi c\hbar}\frac{1}{6}\sum_{\nu}\frac{1}{M_F}\sum_{M}\sum_{\vec{q}}|T_{M\nu}^{fi}|^2d\Omega, \quad (40)$$

where

$$T_{M\nu}^{fi}=\sum_{j}\frac{\langle M,f|\hat{H}_{\text{eph}}|j\rangle\langle j|\vec{e}_{\vec{Q}}\hat{\vec{p}}|\nu,i\rangle}{E_i-E_j}. \quad (41)$$

Here, $\hat{\vec{p}}$ is the momentum operator, $\hat{H}_{\text{eph}}$ is the electron-phonon interaction Hamiltonian, $\vec{e}_{\vec{Q}}$ is the light polarization vector perpendicular to the light propagation direction $\vec{Q}$, and c is the speed of light in vacuum. The effective refraction index n_{eff} for radiative recombination of carriers confined in Si nanocrystals embedded in some media with a dielectric constant κ_{m} is given by[42]

$$n_{\text{eff}}=\left(\frac{\kappa_{\text{m}}}{\kappa_{\text{eff}}}\right)^2\kappa_{\text{m}}^{1/2}, \quad (42)$$

where $\kappa_{\text{eff}}=(\kappa_{\text{Si}}+2\kappa_{\text{m}})/3$. We have also taken into account the degeneracy, $M_F=2F+1$, of the hole state (we can neglect the spin degeneracy) and degeneracy, 6, of the electron state (we do not consider electron states having an azimuthal quantum number different from zero and also neglect the spin degeneracy).

In silicon, only the holes interact with optical phonons due to deformation potentials. Thus the transition goes via a virtual state belonging to the valence band. The energy distance between the conduction and valence bands at the point $\vec{k}=\vec{k}_{0,\nu}$ in the Brillouin zone is equal to 4.3 eV, which makes it possible to use the approximation $E_i-E_j\simeq\Delta_i=4.3$ eV and to simplify Eq. (41). Then, after integrating over $d\Omega$ and taking into account two possible polarizations of emitted light, Eq. (40) takes the form

$$P_r^{fi}=\frac{8\pi}{3}\frac{1}{\Delta_i^2}\left(\frac{e}{mc}\right)^2\frac{\omega n_{\text{eff}}}{2\pi c\hbar}\times\frac{1}{6}\sum_{\nu}\frac{1}{M_F}\sum_{M}\sum_{\alpha=x,y,z}|\langle M,f|\hat{H}_{\text{eph}}\hat{p}_\alpha|\nu,i\rangle|^2. \quad (43)$$

The Hamiltonian of the hole interaction with optical phonons, in the case when the spin-orbit interaction is neglected, is given by[12,43]

$$\hat{H}_{\text{eph}}=\frac{2}{\sqrt{3}}\frac{d_0}{a}(v_x\{\hat{J}_y,\hat{J}_z\}+v_y\{\hat{J}_z,\hat{J}_x\}+v_z\{\hat{J}_x,\hat{J}_y\}), \quad (44)$$

where d_0 is the optical-phonon deformation potential. We used $d_0=27$ eV for Si.[44,45] $\{\hat{J}_i,\hat{J}_j\}=\hat{J}_i\hat{J}_j+\hat{J}_j\hat{J}_i$ is the anticommutator of projections of the operator $\hat{\vec{J}}$ introduced in Sec. III, and the field of the relative atomic displacement $2\vec{v}$ is given by

$$\vec{v}=\sqrt{\frac{\hbar}{2\rho\omega_0V}}\sum_{\vec{q},\sigma}\vec{e}_{\vec{q},\sigma}(\hat{a}_{\vec{q},\sigma}e^{i\vec{q}\vec{r}}+\hat{a}_{\vec{q},\sigma}^{\dagger}e^{-i\vec{q}\vec{r}}). \quad (45)$$

Here, $\hat{a}_{\vec{q},\sigma}^{\dagger}$ and $\hat{a}_{\vec{q},\sigma}$ are creation and annihilation operators of a phonon having wave vector $\vec{q}$ and polarization σ, ω_0 is the optical-phonon frequency, ρ is the mass density, and V is the normalization volume. We have neglected the small difference in the frequency of LO and TO phonons.

Let us consider only the z valley for the electron initial state ($\nu=z$), taking into account that the others give the same contribution. Then one can use for the phonon polarization that $\vec{q}\approx\vec{k}_{0,z}$, i.e., the vector $\vec{q}$ is along the z axis. So, transversal phonon polarizations $\vec{e}_{\text{TO1}}$ and $\vec{e}_{\text{TO2}}$ can be chosen to be directed along the x and y axes ($\vec{e}_{\text{TO1}}=\vec{e}_x$, $\vec{e}_{\text{TO1}}=\vec{e}_y$), while the longitudinal $\vec{e}_{\text{LO}}$ one is directed along the z axis ($\vec{e}_{\text{LO}}=\vec{e}_z$). The temperature is assumed to be low enough ($kT\ll\hbar\omega_0$) to neglect absorption of phonons. Then for a given phonon polarization $\vec{e}_\sigma$, the whole $\hat{H}_{\text{eph}}$ can be replaced with

$$\frac{2}{\sqrt{3}}\frac{d_0}{a}\sqrt{\frac{\hbar}{2\rho\omega_0V}}\hat{J}_L\sum_{\vec{q}}e^{-i\vec{q}\vec{r}}, \quad (46)$$

where

$$\hat{J}_L=e_{\sigma,x}\{\hat{J}_y,\hat{J}_z\}+e_{\sigma,y}\{\hat{J}_z,\hat{J}_x\}+e_{\sigma,z}\{\hat{J}_x,\hat{J}_y\}. \quad (47)$$

We see that the first two terms on the right hand side give contributions from TO phonons and the last term gives contribution from LO phonons.

Using Eq. (46) in Eq. (43) and taking into account that the electron and hole envelope functions vary in space more slowly than the corresponding Bloch amplitudes, we come to the following result:

$$P_r^{fi}=\frac{8}{9}\frac{d_0^2e^2\omega n_{\text{eff}}}{a^2m_0^2c^3\rho\omega_0\Delta_i^2}\frac{1}{M_F}\sum_{M}\sum_{\alpha=x,y,z}M_{\alpha,z}^{M}, \quad (48)$$

where

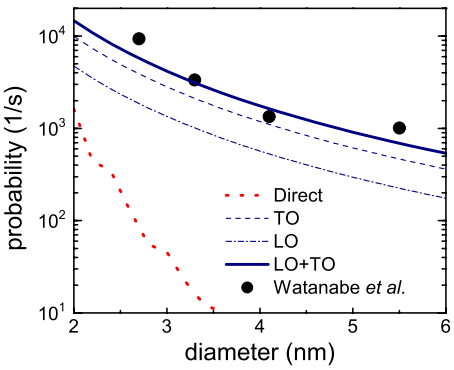

FIG. 5. (Color online) Probabilities $P_{r,gr}$ of radiative transitions between the ground electron and hole states assisted by emission of a TO phonon (dashed line), an LO phonon (dash-dot line), and their sum (thick solid line) as well as the probability of direct (zero phonon) transition (dot line), as functions of nanocrystal diameter. Experimental points (Ref. 40) are shown as well.

$$M^M_{\alpha,z} = \sum_{m_1,m_2,m,m'} \langle u_{m_1}|\hat{J}_L|u_m\rangle\langle u_m|\hat{p}_\alpha|u_{cz}\rangle \times \langle u_{m_2}|\hat{J}_L|u_{m'}\rangle^*\langle u_{m'}|\hat{p}_\alpha|u_{cz}\rangle^* \times \int d^3r|\xi^e_i(\vec{r})|^2\psi^{M*}_{m_1}(\vec{r})\psi^M_{m_2}(\vec{r}). \quad (49)$$

Here, $\xi^e_i(\vec{r})$ is the electron envelope function in the initial state, and for brevity of notation, the total hole wave function in the final state is written as $\psi^{h,f}_{FM}(\vec{r})=\Sigma_m\psi^M_m(\vec{r})u_m$ [cf. Eqs. (9)–(12)]. Calculating matrix elements (49), one should take into account that only the nonzero matrix elements of the momentum operator projections are

$$\langle u_\pm|\hat{p}_y|u_{cz}\rangle = \pm\langle u_\pm|\hat{p}_x|u_{cz}\rangle = \frac{1}{\sqrt{2}}p_{cv}, \quad (50)$$

and p_{cv} was calculated in Ref. 18.

The results of calculations for the ground exciton state ($P_{r,gr}$) are presented in Fig. 5. The probabilities of radiative transitions involving excited states P_r have similar dependences on the nanocrystal size, being of the same order of magnitude (e.g., for the transition from the second electron state to the first hole state, $P_r \approx 0.8P_{r,gr}$). In Fig. 5, the result of calculations of direct (zero phonon) radiative transition for the ground exciton state is presented as well. The probability of the direct optical transition was calculated using the first order perturbation theory, leading to

$$P^{fi}_{r,\mathrm{dir}} = \frac{4}{3}\frac{e^2\omega n_{\mathrm{eff}}}{m_0^2c^3\hbar}\frac{1}{M_F}\sum_M |p^M_{\mathrm{ex}}|^2, \quad (51)$$

where the matrix element p^M_{ex} is given by

$$p^M_{\mathrm{ex}} = \sum_m \langle u_m|\hat{\vec{p}}|u_{cz}\rangle \int d^3r\xi^e_i(\vec{r})\psi^{M*}_m(\vec{r})e^{ik_{0z}}. \quad (52)$$

Such a transition becomes possible for confined carriers, but one can see that for quantum dots with a diameter larger than 2 nm, the corresponding oscillator strength is noticeably smaller than in the case of transitions assisted by emission of an optical phonon. This is a well-known experimental fact.[46] One should notice that the shown probability of the direct radiative transition has been calculated as an average value over the nanocrystal size distribution (±0.15 nm here) in order to achieve an acceptable convergence of the numerical integration and to avoid strong oscillations of the result.[47,48] One can see from Fig. 5 that our results reproduce the experimental data on radiative lifetimes in Si/SiO_2 nanocrystals[40] very well. As far as radiative transitions most probably take place together with a phonon emission, the exciton band gap derived from the photoluminescence spectra should generally be lower than the calculated one by the amount of the phonon energy (cf. Fig. 4).

VI. CONCLUSION

We have calculated the wave functions and the energy levels of confined carriers in Si quantum dots inside a SiO_2 matrix as functions of the dot diameter. It has been shown that for small quantum dots ($d \lesssim 2.5$ nm), the energy spacing between neighboring electron and hole levels is of the order of hundreds of meV, and for electrons they are larger than those for holes. Such energy spacings are also larger than the energy-level splittings due to different mechanisms[9] which are not accounted for in this paper. Therefore, the single-phonon relaxation between the levels becomes impossible and the time of relaxation of hot carriers to the ground state increases. The calculated recombination energies of an electron-hole pair in the ground state and the probabilities of radiative interband transitions between the ground electron and hole levels are in good agreement with experimental data. Comparison of the electron and hole levels calculated by our method and by state-of-the-art computational methods[8,17] could lead, in the future, to a more rigorous formulation of the boundary conditions in the framework of the multiband effective mass approximation. This would allow us to produce quantitative calculations of processes involving electrons and holes in Si nanocrystals with a reasonable computational effort.

ACKNOWLEDGMENTS

We thank E. L. Ivchenko and V. I. Perel for useful discussions. On the Russian side, this work was partly financially supported by RFBR, NWO, INTAS, and RAS. One of the authors (A.A.P.) was also supported by the Dynasty Foundation.

APPENDIX: EQUATIONS FOR QUANTIZATION ENERGIES OF HOLES

The equations determining the energy quantization levels in the cases of mixed, heavy, and light hole types are

$$\left\{\nu\kappa\left[\frac{F-1}{2F-1}\frac{k_{F-2}(\kappa)}{k_{F-1}(\kappa)}+\frac{F}{2F-1}\frac{k_F(\kappa)}{k_{F-1}(\kappa)}\right]j_{F-1}(\lambda)+\left(1+\frac{F-1}{2F+1}\mu\right)\lambda\left[\frac{F-1}{2F-1}j_{F-2}(\lambda)-\frac{F}{2F-1}j_F(\lambda)\right]\right.$$
$$\left.+\mu\left[\frac{3}{2}\frac{F-1}{2F+1}j_{F-1}(\lambda)+\frac{3F(F+2)}{2F+1}j_{F+1}(\lambda)\right]+\frac{3F}{2F+1}\mu\lambda\left[\frac{F+1}{2F+3}j_F(\lambda)-\frac{F+2}{2F+3}j_{F+2}(\lambda)\right]\right\}\left\{\frac{F+1}{F}\nu\kappa\left[\frac{F+1}{2F+3}\frac{k_F(\kappa)}{k_{F+1}(\kappa)}\right.\right.$$
$$\left.+\frac{F+2}{2F+3}\frac{k_{F+2}(\kappa)}{k_{F+1}(\kappa)}\right]j_{F+1}(\lambda\beta)-3\frac{F+1}{2F+1}\mu\lambda\beta\left[\frac{F-1}{2F-1}j_{F-2}(\lambda\beta)-\frac{F}{2F-1}j_F(\lambda\beta)\right]+\mu\left[\frac{3(F^2-1)}{2F+1}j_{F-1}(\lambda\beta)\right.$$
$$\left.\left.+\frac{3}{2}\frac{(F+1)(F+2)}{F(2F+1)}j_{F+1}(\lambda\beta)\right]+\frac{F+1}{F}\left(1+\frac{F+2}{2F+1}\mu\right)\lambda\beta\left[\frac{F+1}{2F+3}j_F(\lambda\beta)-\frac{F+2}{2F+3}j_{F+2}(\lambda\beta)\right]\right\}$$
$$=\left\{\nu\kappa\left[\frac{F-1}{2F-1}\frac{k_{F-2}(\kappa)}{k_{F-1}(\kappa)}+\frac{F}{2F-1}\frac{k_F(\kappa)}{k_{F-1}(\kappa)}\right]j_{F-1}(\lambda\beta)+\left(1+\frac{F-1}{2F+1}\mu\right)\lambda\beta\left[\frac{F-1}{2F-1}j_{F-2}(\lambda\beta)-\frac{F}{2F-1}j_F(\lambda\beta)\right]\right.$$
$$\left.+\mu\left[\frac{3}{2}\frac{F-1}{2F+1}j_{F-1}(\lambda\beta)-\frac{3(F+1)(F+2)}{2F+1}j_{F+1}(\lambda\beta)\right]-\frac{3(F+1)}{2F+1}\mu\lambda\beta\left[\frac{F+1}{2F+3}j_F(\lambda\beta)-\frac{F+2}{2F+3}j_{F+2}(\lambda\beta)\right]\right\}$$
$$\times\left\{-\nu\kappa\left[\frac{F+1}{2F+3}\frac{k_F(\kappa)}{k_{F+1}(\kappa)}+\frac{F+2}{2F+3}\frac{k_{F+2}(\kappa)}{k_{F+1}(\kappa)}\right]j_{F+1}(\lambda)-\frac{3(F+1)}{2F+1}\mu\lambda\left[\frac{F-1}{2F-1}j_{F-2}(\lambda)-\frac{F}{2F-1}j_F(\lambda)\right]\right.$$
$$\left.+\mu\left[\frac{3(F^2-1)}{2F+1}j_{F-1}(\lambda)-\frac{3}{2}\frac{F+2}{2F+1}j_{F+1}(\lambda)\right]-\left(1+\frac{F+2}{2F+1}\mu\right)\lambda\left[\frac{F+1}{2F+3}j_F(\lambda)-\frac{F+2}{2F+3}j_{F+2}(\lambda)\right]\right\},\tag{A1}$$

$$(1-\mu)\lambda\left[\frac{F}{2F+1}j_{F-1}(\lambda)-\frac{F+1}{2F+1}j_{F+1}(\lambda)\right]-\frac{3}{2}\mu j_F(\lambda)+\nu\kappa j_F(\lambda)\left[\frac{F}{2F+1}\frac{k_{F-1}(\kappa)}{k_F(\kappa)}+\frac{F+1}{2F+1}\frac{k_{F+1}(\kappa)}{k_F(\kappa)}\right]=0,\tag{A2}$$

$$(1+2\mu)\lambda\beta[j_0(\lambda\beta)-2j_2(\lambda\beta)]k_1(\kappa)+9\mu j_1(\lambda\beta)k_1(\kappa)+\eta\kappa j_1(\lambda\beta)[k_0(\kappa)+2k_2(\kappa)]=0,\tag{A3}$$

respectively. Here, $\mu=B/A$, $\nu=A_0/A$, β is defined by Eq. (17), and λ and κ are functions of the hole energy E determined by Eqs. (18) and (23) respectively.

*Also at Ioffe Physico-Technical Institute of RAS, 26 Polytechnicheskaya, 194021 St. Petersburg, Russia; andrey.moskalenko@physik.uni-halle.de

[1] L. Pavesi, L. Dal Negro, C. Mazzoleni, G. Franzo, and F. Priolo, Nature (London) **440**, 408 (2000).

[2] A. Polman, Nat. Mater. **1**, 10 (2002).

[3] J. P. Proot, C. Delerue, and G. Allan, Appl. Phys. Lett. **61**, 1948 (1992).

[4] E. Martin, C. Delerue, G. Allan, and M. Lannoo, Phys. Rev. B **50**, 18258 (1994).

[5] B. Delley and E. F. Steigmeier, Phys. Rev. B **47**, 1397 (1993).

[6] L.-W. Wang and A. Zunger, J. Chem. Phys. **100**, 2394 (1994).

[7] M. V. Wolkin, J. Jorne, P. M. Fauchet, G. Allan, and C. Delerue, Phys. Rev. Lett. **82**, 197 (1999).

[8] C. S. Garoufalis and A. D. Zdetsis, Phys. Chem. Chem. Phys. **8**, 808 (2006).

[9] Y. M. Niquet, C. Delerue, G. Allan, and M. Lannoo, Phys. Rev. B **62**, 5109 (2000).

[10] V. A. Burdov, JETP **94**, 411 (2002).

[11] I. Izeddin, A. S. Moskalenko, I. N. Yassievich, M. Fujii, and T. Gregorkiewicz, Phys. Rev. Lett. **97**, 207401 (2006).

[12] P. Yu and M. Cardona, *Fundamentals of Semiconductors. Physics and Material Properties*, 3rd ed. (Springer, Berlin, 2001).

[13] E. L. Ivchenko and G. E. Pikus, *Superlattices and Other Heterostructures* (Springer, Berlin, 1997).

[14] A. Dargys and J. Kundrotas, *Handbook on Physical Properties of Ge, Si, GaAs and InP* (Science and Encyclopedia Publishers, Vilnius, 1994).

[15] V. A. Burdov, Semiconductors **36**, 1154 (2002).

[16] S. M. Sze, *Physics of Semiconductor Devices* (Wiley, New York, 1981).

[17] M. Luppi and S. Ossicini, Phys. Rev. B **71**, 035340 (2005).

[18] M. Cardona and F. H. Pollak, Phys. Rev. **142**, 530 (1966).

[19] V. N. Abakumov, V. I. Perel, and I. N. Yassievich, in *Nonradiative Recombination in Semiconductors*, edited by V. M. Agranovich and A. A. Maradudin, Modern Problems in Condensed Matter Sciences Vol. 33 (Elsevier, Amsterdam, 1991).

[20] A. R. Edmonds, *Angular Momentum in Quantum Mechanics* (Princeton University Press, Princeton, NJ, 1957).

[21] A. Baldereschi and N. O. Lipari, Phys. Rev. B **8**, 2697 (1973).

[22] D. A. Varshalovich, A. N. Moskalev, and V. K. Khersonskii, *Quantum Theory of Angular Momentum* (World Scientific, Sin-

gapore, 1988).
[23] J. R. Chelikowsky and M. Schlüter, Phys. Rev. B **15**, 4020 (1977).
[24] *Handbook of Mathematical Functions*, edited by M. Abramowitz and I. A. Stegun (Dover, New York, 1972).
[25] E. Hendry, M. Koeberg, F. Wang, H. Zhang, C. de Mello Donega, D. Vanmaekelbergh, and M. Bonn, Phys. Rev. Lett. **96**, 057408 (2006).
[26] Al. L. Efros and A. L. Efros, Fiz. Tekh. Poluprovodn. (S.-Peterburg) **16**, 1209 (1982) [Sov. Phys. Semicond. **16**, 772 (1982)].
[27] L. E. Brus, J. Chem. Phys. **80**, 4403 (1984).
[28] M. Lannoo, C. Delerue, and G. Allan, Phys. Rev. Lett. **74**, 3415 (1995).
[29] A. S. Moskalenko and I. N. Yassievich, Phys. Solid State **46**, 1508 (2004).
[30] L. Banyai, P. Gilliot, Y. Z. Hu, and S. W. Koch, Phys. Rev. B **45**, 14136 (1992).
[31] A. Franceschetti and A. Zunger, Phys. Rev. B **62**, 2614 (2000).
[32] P. G. Bolcatto and C. R. Proetto, J. Phys.: Condens. Matter **13**, 319 (2001).
[33] C. Delerue, M. Lannoo, and G. Allan, Phys. Rev. Lett. **84**, 2457 (2000).
[34] M. Bruno, M. Palummo, A. Marini, R. Del Sole, and S. Ossicini, Phys. Rev. Lett. **98**, 036807 (2007).
[35] E. Luppi, F. Iori, R. Magri, O. Pulci, S. Ossicini, E. Degoli, and V. Olevano, Phys. Rev. B **75**, 033303 (2007).
[36] I. N. Yassievich, A. S. Moskalenko, and A. A. Prokofiev, Mater. Sci. Eng., C **27**, 1386 (2007).
[37] Y. Kanzawa, T. Kageyama, S. Takeda, M. Fujii, S. Hayashi, and K. Yamamoto, Solid State Commun. **102**, 533 (1997).
[38] S. Guha, B. Qadri, R. G. Musket, M. A. Wall, and T. Shimizu-Iwayama, J. Appl. Phys. **88**, 3954 (2000).
[39] S. Takeoka, M. Fujii, and S. Hayashi, Phys. Rev. B **62**, 16820 (2000).
[40] K. Watanabe, M. Fujii, and S. Hayashi, J. Appl. Phys. **90**, 4761 (2001).
[41] G. Hadjisavvas and P. C. Kelires, Phys. Rev. Lett. **93**, 226104 (2004).
[42] A. Thränhardt, C. Ell, G. Khitrova, and H. M. Gibbs, Phys. Rev. B **65**, 035327 (2002).
[43] G. E. Pikus and G. L. Bir, *Symmetry and Strain-induced Effects in Semiconductors* (Wiley, New York, 1974).
[44] L. Brey, N. E. Christensen, and M. Cardona, Phys. Rev. B **36**, 2638 (1987).
[45] A. Blacha, H. Presting, and M. Cardona, Phys. Status Solidi B **126**, 11 (1984).
[46] D. Kovalev, H. Heckler, M. Ben-Chorin, G. Polisski, M. Schwartzkopff, and F. Koch, Phys. Rev. Lett. **81**, 2803 (1998).
[47] M. S. Hybertsen, Phys. Rev. Lett. **72**, 1514 (1994).
[48] C. Delerue, G. Allan, and M. Lannoo, Phys. Rev. B **64**, 193402 (2001).
[49] Due to limitations of our method, we can expect only very qualitative results for very small nanocrystals having the number of Si atoms less than the order of 100.